Journal of Aeronautics, Astronautics and Aviation, Vol. 51, No. 1, pp. 031 - 042 (2019)
DOI: 10.6125/JoAAA.201903_51(1).03

Plasma Behavior in a Solid-Fed Pulsed Plasma Thruster *

Yueh-Heng Li [1**], Sunil Palagiri [1], Po-Yu Chang [2], Christoph Montag [3], and Georg Herdrich [3]

[1]*Department of Aeronautics and Astronautics, National Cheng Kung University, Tainan, 70101, Taiwan.*
[2]*Institute of Space and Plasma Sciences, National Cheng Kung University, Tainan, 70101, Taiwan.*
[3]*Institute of Space Systems, University of Stuttgart, Stuttgart, 70569, Germany.*

ABSTRACT

This paper describes plasma acceleration behavior in a pulsed plasma thruster (PPT). A PPT is a form of electric propulsion device in which plasma is accelerated by the interaction between pulse currents and magnetic fields to create thrust. It is one of the most promising electric propulsion devices with the advantages of simplicity and relatively low manufacturing cost. In this study, a prototype solid-fed PPT that produces plasma and accelerates it to a high velocity was designed and demonstrated. This prototype PPT produces an impulse bit of 84 μN·s when 6.25 J of energy is employed. Plasma is a quasi-neutral matter of charged and neutral particles that exhibits a collective behavior. To examine plasma behavior, a triple Langmuir probe was designed to determine the electron density and electron velocity. A plasma density of 8×10^{20} m^{-3}, 30 mm from a nozzle with a maximum electron velocity of 25 km/s, was observed. In addition, a high-speed camera was employed to visualize the Lorentz force acting on the plasma and the evolution of plasma plume formation in the discharge chamber.

Keywords: Electric Propulsion, Pulsed Plasma Thruster, Langmuir triple probe, Plasma density.

NOMENCLATURE

D_i	Diameter of probe (mm)
E	Energy stored in capacitor (J)
h	Electrode gap (mm)
I	Current (A)
I_{bit}	Impulse bit (N•s)
I_{es}	Electron saturation current (A)
I_{is}	Ion saturation current (A)
I_{px}	Current collected by Probe x (1, 2, 3) (A)
I_{SP}	Specific impulse (s)
K	Boltzmann constant

* Manuscript received, August 5, 2018, final revision, October 11, 2018
** To whom correspondence should be addressed, E-mail: yueheng@mail.ncku.edu.tw

l	Electrode length (mm)
L_p	Probe length (mm)
m_i	Mass of ion (kg)
n_e	Electron density ($1/m^3$)
n_i	Ion density ($1/m^3$)
P	Power (W)
Q, q	Charge (C)
R	Resistance (Ω)
Rp	Probe resistance (Ω)
S_p	Area of the probe (mm)
t	Time (s)
T_e	Electron temperature (K)
V	Voltage (V)
V_c	Capacitor charging voltage (V)
V_{d1-3}	Potential difference between Probe 1 and Probe 3 (V)
V_e	Exit Velocity
V_o	Voltage output (V)
V_x	Voltage of Probe x (1, 2, 3) (V)
w	Electrode width (mm)
μ	Magnetic permeability (H/m)

I. INTRODUCTION

NASA's recent announcement of its intention to return to the Moon, visit Mars, and seek out new worlds has led to new interest in advanced propulsion. Several concepts, including nuclear thermal rockets, solar thermal sails, and electric thrusters, are under development for satellites and deep-space missions. Of the many types of nonchemical thruster, electrical thrusters are one of the few currently in use. Their relatively simple design and high specific impulse make them excellent candidates for satellite maneuvers, orbital station-keeping, and deep-space exploration. However, the pulsed plasma thruster's (PPT's) simplicity and relatively low cost make it the most excellent candidate, and researchers aspire to adopt it for satellite programs. PPTs operate by discharging stored energy into some form of propellant located between two electrodes. The initial input of energy from an external device ionizes the propellant, forming low-resistance plasma that electrically connects the capacitor to the electrodes, allowing it to discharge. High currents induced by low resistance create strong magnet fields within the electrodes. Energy released by the capacitor is used to ionize further propellant, creating additional plasma. The cross product between the current density flowing through the plasma and the magnetic fields creates a force (i.e., the Lorentz force) that accelerates the plasma bulk along the axis of the thruster. The coupled inductance–capacitance–resistance (LCR) system creates a multipulse plasma discharge of the order of tens of microseconds. The complete process is repeated regularly, ultimately leading to exploitable thrust produced by a satellite's propulsion module.

The PPT comprises several hardware components: the power unit (to transfer power from the spacecraft bus and convert it into a high-voltage line), energy storage device (to provide energy to the plasma discharge), discharge chamber (to allow energy to flow from the storage device into the plasma), discharge initiator (to initiate the discharge by introducing electrons), and propellant (to provide the mass to the plasma, which is accelerated in the discharge chamber). The PPT's discharge chamber comprises the empty space and components that are involved in the acceleration of the plasma that is created within it. Originally, the parallel plate electrodes maximized the electromagnet acceleration effects, and the coaxial electrodes maximized the electrothermal acceleration effects. However, Keidar et al. [1] demonstrated that even when a coaxial electrode configuration is used, the primary acceleration mechanism was electromagnetic acceleration. Kamhawi et al. [2] ascertained that electrode geometry had a significant effect on the impulse bit. Maximizing the ratio of the electrode separation distance to the electrode width had the most substantial effect. Nawaz et al. [3] discovered that when electrode separation increased, both the mass bit and impulse bit increased, but the exhaust velocity decreased. When the width of the electrodes was reduced, an optimum was identified. Furthermore, flared electrode use increased the impulse bit and exhaust velocity. The erosion rate of the electrode materials in the discharge chamber was investigated. Multifarious materials are used for the anode, but the cathode is invariably Cu [4]. The PPT was discharged for approximately 100,000 pulses, and the total electrode mass loss was measured and subsequently averaged to provide the mass loss per discharge. The most significant result was that the mass loss per discharge varied depending on the anode material. At the longest length (17.3 cm), no particulate or crater formation was observed on the electrode surface through scanning electron microscopy. Tamura et al. [5] discharged 500,000 pulses through a 1-μF capacitor at 2.37 and 3.59 J for brass and molybdenum electrodes, respectively. The results indicated that electrode material selection had no effect on PPT performance. Furthermore, Laystrom et al. [6] reported that the geometry of the anode tip had an effect on the anode mass loss because it varied between 0.0423 and 0.261 μg/J. The optimal design was a truncated cone. Truncated-tip anodes made from Elkonite (90% W and 10% Cu), pure W, and Glidcop (98.9% Cu, 0.6% Al, and trace Fe and Pb) were experimented on. Elkonite had the highest erosion rate (0.41 μg/J); W had the lowest (0.12 μg/J).

The discharge initiator is the device that somehow introduces charged particles into the discharge chamber. This augments the electric field to such an extent that a breakdown between the electrodes occurs. In a PPT, this role is commonly fulfilled using a spark plug. The life-limiting characteristic of spark plugs meant that they accumulated 38 million pulses in total [7]. In addition, the sparkplug that was used consistently failed between pulse Nos. 1 to 4 million because Teflon-derived fluorocarbon deposition formed on its surface. The cleaning process revealed that the outer nickel electrode was subject to significant erosion; thus, electrodes with both inner and outer electrodes made from Ir were developed [7]. Alternatively, to mitigate the aforementioned shortcomings, a laser-assisted discharge initiator was proposed. Cooley and Choueiri [8] used an Nd:YAG laser with a fundamental wavelength of 1064 nm to ignite a gas-fed PPT with Ar propellant at 2 Torr. Kawakami et al. [9] performed PPT initiation tests by using an Nd:YAG laser with a fundamental wavelength of 1064 nm, a fixed pulse energy of 220 mJ per pulse, and a pulse width of 10 ns.

The plasma produced in the discharge chamber requires mass. This is provided by the propellant that is introduced into the discharge chamber. All flown PPTs have used Teflon as a propellant source. Teflon is an inert substance with few outgassing properties in a vacuum. As the PPT discharges, the Teflon is eroded nonuniformly, which creates a commonly observed indentation in the Teflon surface. Scharlemann and York [10] proposed a hybrid liquid–solid system in which water would uniformly diffuse into the propellant. Water was introduced to provide a path of less resistance; thus, the energy could be distributed over the entire propellant surface. In addition, solid Teflon is fabricated using long carbon polymer chains; when broken down in the discharge, the carbon locked in these chains coats the thruster housing. If the carbon accumulated, it would create an electrical path between the electrodes that would cause tracking that would lead to the thruster failing. Low-carbon propellants, including purified water, methanol, ethanol, and butanol, were used to extend the thruster's operating time [11, 12].

The simplicity of constructing a PPT contrasts with the complexity of understanding the discharge process. The discharge process occurs on a microsecond timescale but certain effects and formations occur on a nanosecond timescale. Two periods constitute the discharge process: the first is when the plasma is in the discharge chamber and is created and accelerated. The second is when the plasma is expelled from the chamber and forms a plasma plume. Several nonintrusive measurement techniques have been used to study the first period. Researchers have applied laser interferometry measurements to ascertain electron density [13], spectroscopic emission measurements to record the light emissions from the plasma mass's constituent parts [14], and high-speed photography to image the discharge process on a nanosecond time scale [15, 16]. For the second period, once the plasma has been expelled from the discharge chamber, more intrusive measurement processes are used. Retarding field energy analyzers (RFEAs) use multiple charged grids to detail the plasma plume's ion composition [17]. Current-mode triple and quadruple Langmuir probes measure the electron temperature [18], electron density, and ratio of ion speed to the most probable thermal speed in the plasma plume. The RFEA and Langmuir probes can also act as a time of flight (ToF) probe to measure the speed of the fastest ions from the discharge chamber to the probe heads [15].

To help Taiwan's researchers explore the celestial sphere, an appropriate electric propulsion is imperative. The PPT is widely known among researchers; however, it

is often underestimated because of its simplicity and relatively low manufacturing costs. Low energy conversion efficiency ratings from electrical to kinetic energy and the yet-to-be-achieved goal to increase this value to more than 20% in conventional designs have limited the PPT's acceptance by industry. Despite its simple and cost-effective production, the PPT has complex underlying principles. This study attempted to develop a reliable and compact solid-fed PPT (S-PPT) prototype. To characterize the properties of plasma, a triple Langmuir probe was developed and fabricated to measure the plasma's electron density, and a high-speed camera was employed to assess PPT discharge evolution within the discharge chamber. Ultimately, the theoretical thruster and maximum electron velocity of the proposed S-PPT were characterized.

1.1 Operational process of solid-fed pulsed plasma thruster

The S-PPT's operational process [19] can be divided into four stages: preignition, ignition, discharge, and acceleration (Figure 1).

*1. **Preignition**:* The process commences with the power unit supplying electrical energy to the capacitor. The capacitor has a dielectric medium between the plates, and as the capacitor charges, the dielectric molecules realign to the applied electric field, which augments the capacitor's surface charge. The charging time depends on the resistor and capacitance of the capacitor. Once the required amount of energy is stored in the capacitor, the second stage can commence.

*2. **Initiation**:* After the capacitor is charged, a spark plug creates a spark between the inner and outer electrodes of the electrodes; the resultant spark releases the electrons to create a plasma source between the main electrodes.

*3. **Discharge**:* While the plasma source forms between the electrodes, the plasma source acts as a conductive path between the electrodes and creates a current loop. Because the discharge time is short (of the order of several microseconds), a high instantaneous current (of the order of several kiloamperes) is generated. This high current ablates more Teflon, induces ionization, and generates a plasma plume.

*4. **Acceleration**:* The large current in the plasma plume induces a strong magnetic field. Current in the presence of the magnetic field experiences a Lorentz (J × B) force. This force accelerates plasma plume release from the thruster at a high speed, and nonionized particles are expanded from the thruster at a low speed.

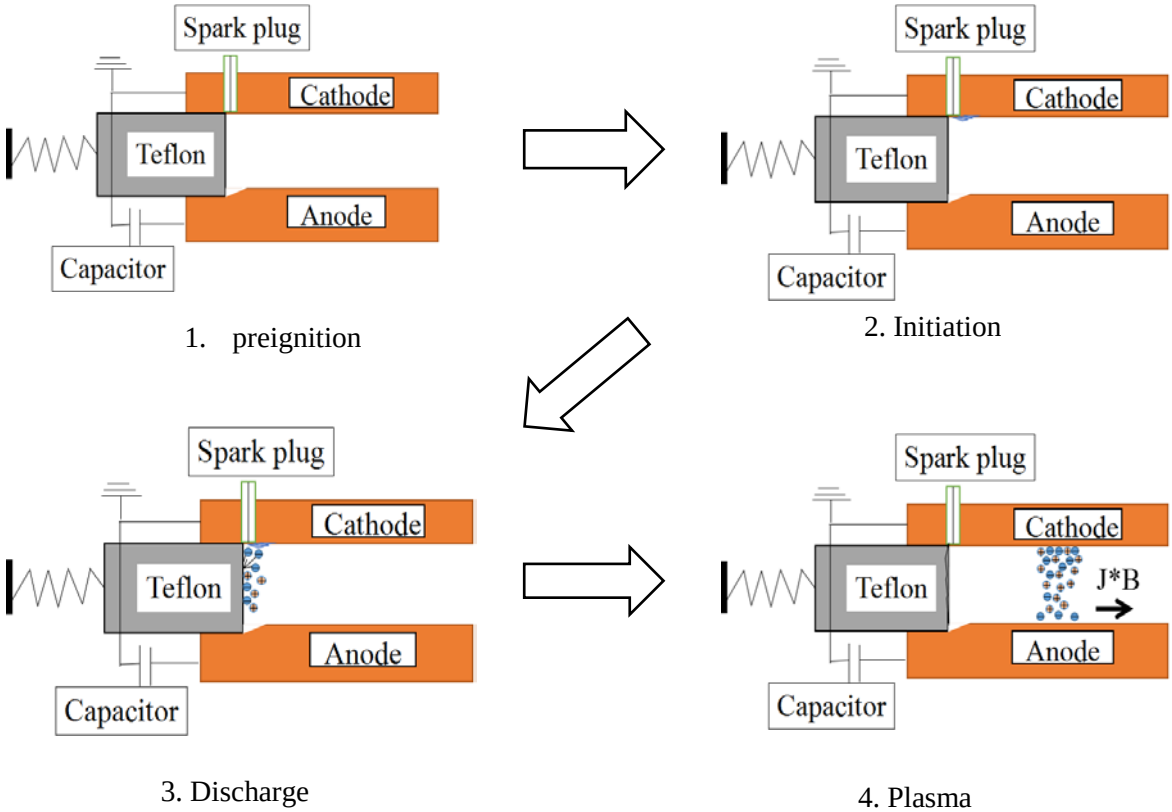

Figure 1 The operational process of S-PPT.

1.2. Plasma behavior

Plasma behavior is an essential factor to consider when implementing or optimizing PPT for space missions. Not a solid, liquid, or gas, plasma is considered the fourth fundamental state of matter. When a solid is heated, it melts and become a liquid. When a liquid is heated, it boils and becomes a gas; in turn, when a gas is heated, it becomes ionized, and the ionized gas, along with the neutral particles, is called plasma. Plasma is defined as a quasi-neutral gas of charged and neutral particles which exhibit a collective behavior [20]. When the charged particles move in the presence of uniform electric and

magnetic fields, they experience J × B force and tend to drift perpendicular to both electrical and magnetic field directions (Figure 1). The properties of the plasma that exits the thruster at a high speed can be measured using a triple probe.

By inserting a probe with the direction of plasma exit as a probe with a properly assigned sweeping voltage. The difference between the plasma potential and probe potential would induce a net current increase or decrease into or out of the probe. On the basis of the induced probe current, the plasma density can be estimated [21]. On the basis of the probe number, it can be classified as one of several types. The three commonest types include the single Langmuir probe, double Langmuir probe, and triple Langmuir probe. The single and double Langmuir probes require a sweeping voltage, which benefits stable plasma (e.g., a flame). However, a time-resolved probe should be used for the PPT because the plasma varies and persists for short durations. Thus, a triple Langmuir probe is used because it uses a bias voltage instead of a sweeping voltage. Eckman et al. [22] used a triple Langmuir probe and concluded that an increase in discharge energy results in higher electron densities but not a higher temperature. Furthermore, the results confirmed that PPT plumes are nonsymmetrical. Schonerr et al. [23] reported that more energy is used in ionization (i.e., a higher excitation or ionization state) rather than ablation (i.e., a higher number density). Gagne et al. [24] opined that the position of the probe should be considered because the density is not identical at all points. Finally, the plasma in the PPT ranges 1×10^{19} to 1×10^{22}. Markusic et al. [25] determined that the current sheet propagates at highly canted angles. They discussed that ion conduction current, electrode erosion, magnetic field asymmetry, and the Hall Effect are discussed as possible causes of this canting.

II. EXPERIMENTAL APPARATUS

2.1 Thruster and facility

A thruster prototype was designed. Teflon is used as the propellant, and the electrodes were fabricated from Cu with a thickness and width of 8 and 10 mm respectively. The electrode gap is 25 mm. A small Cu rod was designed and is insulated from the cathode by using Teflon. This Cu rod acts as the initiator for the thruster. Screws are used for electrodes to connect cables. Quartz is used to support the electrodes and serves as the side walls. PPT is used for the space application; thus, it must be tested in high-vacuum condition before it can operate in space. A small vacuum chamber (diameter: 640 mm; length: 760 mm) was constructed. Although the size of the vacuum chamber is insufficient for major space operations, it is satisfactory for testing micro thrusters. One advantage of its small size is that it requires relatively little time (approximately 10 min) for high-vacuum conditions to be achieved. To create a vacuum in the chamber, a roughing pump is initially used to reduce pressure from 760 to 0.05 Torr; subsequently, a turbo pump is used to attain 10^{-5} to 10^{-6} Torr, which is a high-vacuum condition and sufficient to test thrusters for space applications.

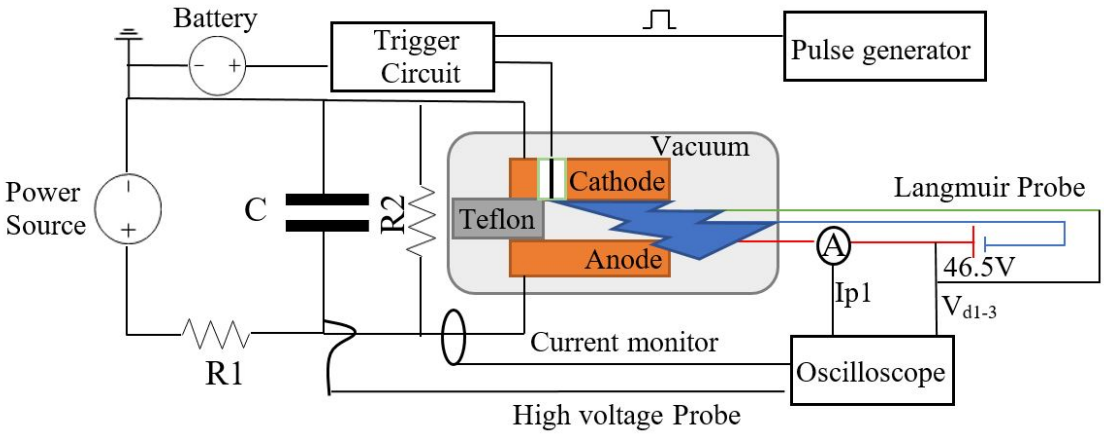

Figure 2 Schematic layout of experimental set up of S-PPT.

To supply power, a trigger circuit that receives 12 V from a battery and converts it to 4 kV is employed as the power processing unit for a spark plug. A 3-W power supply that provides 0–5 kV is used as a power source to charge the 12.5μF capacitor. To protect the power supply from the back current, a resistor (R_1) is used; R_2 is used for safety as shown in Figure 2. If the thruster fails to create discharge, then the energy stored in the capacitor is released through R_2. A high-voltage probe (Tektronix P6015A, 30 kV of maximum voltage) is used to record the PPT capacitor discharge voltage. A current monitor (Pearson Current monitor 301x) with a sensitivity of 0.01 V/A that can measure up to 50 kA of peak discharge current is used to record PPT discharge current pulse. The discharge current curve is used to determine thruster impulse bit.

2.2 Triple Langmuir probe

A triple Langmuir probe is developed to measure the electron density of the plasma. All three probes are made of Chromel and have a diameter D_i of 0.3 mm and a length of 7 mm (Figure 4) To avoid current leakage from the probe and to provide support for the tiny wire, ceramic shielding is applied. The Langmuir triple probe includes

three probes, each with its own role in measurement: Probe 1 is used to collect current from the target plasma while Probe 2 applies a DC bias to the plasma. Probe 3 is left to float; thus, no current flows through it (Figure 2).

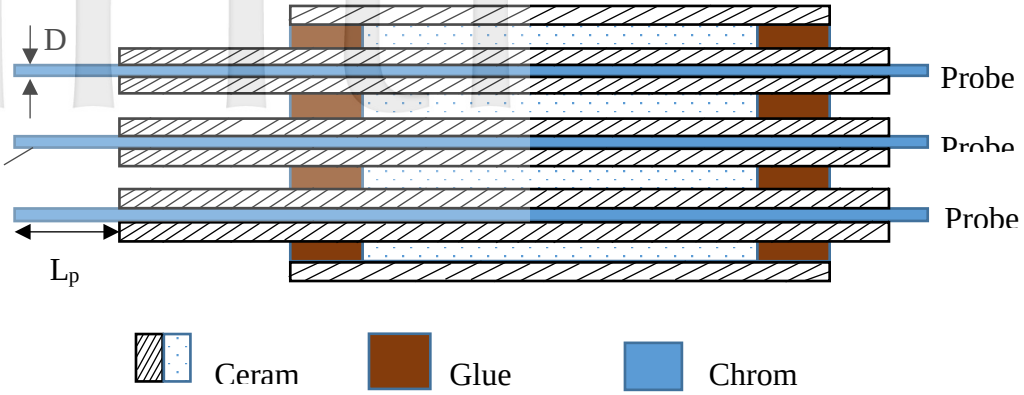

Figure 3 Schematic of Probe Configuration.

The current collected using the probe can contribute to both the electron and ion current [26]; thus, the equation for the current collected by each probe can be written as follows:

$$I_{p1} = I_{is} + I_{es} exp\left(\frac{-eV_1}{KT_e}\right) \quad (1)$$

$$I_{p2} = I_{is} + I_{es} exp\left(\frac{-eV_2}{KT_e}\right) \quad (2)$$

$$I_{p3} = I_{is} + I_{es} exp\left(\frac{-eV_3}{KT_e}\right) \quad (3)$$

With $I_{p1} = -I_{p2}$, $I_{p3} = 0, I_{is} = -I_{es}$ and substituting (1, 2, and 3), we obtain

$$T_e = \frac{e(V_{d1-3})}{Kln2} \quad (4)$$

For ion saturation current, we obtain

$$n_i = n_e = \frac{I_{is}}{qS_p\sqrt{\frac{KT_e}{m_i}}e^{-0.5}} \quad (5)$$

where I_{is} is obtained by subtracting (3) from (1).

$$I_{is} = -I_{p1}\frac{exp\left(\frac{-e(V_{d1-3})}{KT_e}\right)}{1-exp\left(\frac{-e(V_{d1-3})}{KT_e}\right)} \quad (6)$$

Finally, by inserting the result from (6) into (5), we obtain:

$$n_e = \frac{-I_{p1}}{qS_p\sqrt{\frac{KT_e}{m_i}}e^{-0.5}}\frac{exp\left(\frac{-e(V_{d1-3})}{KT_e}\right)}{1-exp\left(\frac{-e(V_{d1-3})}{KT_e}\right)} \quad (7)$$

The current measured by Probe 1 and the potential difference between Probes 1 and 3 provide the plasma plume's current density.

2.3 FASTCAM high-speed camera

To visualize the Lorentz force acting on plasma, a FASTCAM SA5 high-speed camera was used to capture the thruster's discharge process. The FASTCAM SA5 camera had a frame frequency of approximately 300 kHz but at a low resolution (128 × 16 pixels), which cannot capture full thruster. The minimum resolution for capturing the full thruster was 256 × 256. To capture the pictures, 72 kHz with a resolution of (256 × 256) along with an 85-mm Nikon AIS lens (focal ratio: f/1.4) was used. However, the pictures became saturated. To prevent saturation, a 450-nm narrowband optical filter was positioned in front of the high-speed camera.

III. TESTING AND RESULTS

3.1 Effect of energy on impulse bit

A thruster's impulse bit depends on the amount of energy stored in capacitor; the relationship between energy and impulse bit is vital because it defines the thruster's efficiency. During the test, the electrode gap was maintained at 25 mm, but the capacitor charging voltage is increased and tested at different voltages. Increase in voltage will eventually increases changed the energy stored in the capacitor. Table 1 lists all test parameters.

The experimental setup (Figure 2) indicates that although R_2 was used for safety and the high-voltage probe was used to detect voltage, the built-in resistor in the probe and R_2 became part of the circuit, which divided the voltage.

Table 1 Parameters used for energy test.

Parameter	Values
Initiator Voltage	4kV
Electrode Gap (h)	25mm
Capacitor (C)	12.5µf
Charging voltage (V_c)	0.5-2kV
Resistor (R_1)	11MΩ
Resistor (R_2)	100MΩ

This rendered cross-capacitor voltage different to the output voltage from the power supply. To understand this process, a simplified model is displayed in Figure 4. Let resistance in probe be R_p, which is 100 MΩ,

Because R_2 and R_p are in parallel, the equivalent resistance is equal to

$$R_{eq} = \frac{R_2 \times R_p}{(R_2 + R_p)} \quad (8)$$

Now, R_1 and R_{eq} are in series. The voltage between the resistors gives capacitor voltage V_c.

$$V_c = \frac{R_{eq}}{(R_1 + R_{eq})} V_o = \frac{50}{61} V_o \quad (9)$$

To charge the capacitor to 500 V, the power source must provide 610 V. Similarly, for 1000, 1500, and 2000 V, the power source must provide 1220, 1830, and 2440 V, respectively.

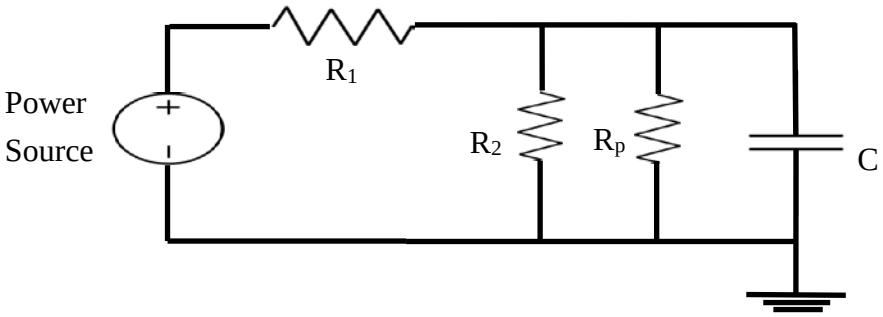

Figure 4 The circuit of voltage divider, while charging capacitor.

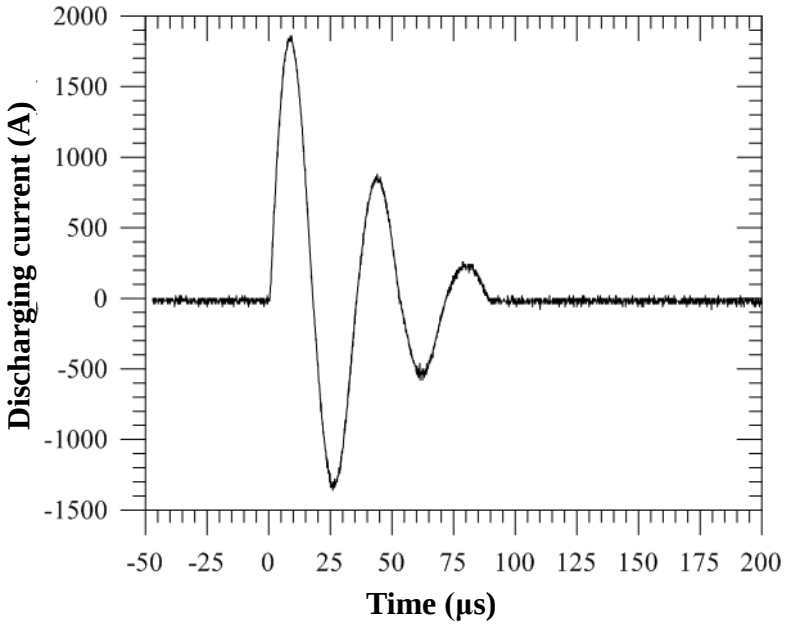

Figure 5 Discharge current with respect to time at 25mm gap.

The capacitor was charged to various voltage, and it was allowed to store different energies.

$$E = \frac{1}{2} c v^2 \quad (10)$$

The impulse bit generated by the Lorentz force is obtained from (11):

$$I_{bit} = \frac{\mu h}{2w} \int_0^\infty i^2 dt \quad (11)$$

The discharge current curve is obtained using the current monitor (Figure 8). Eventually, the discharge current values in (11) provide the impulse bit. The impulse bit is calculated at different energies and plotted in Figure 6.

Figure 6 shows that the impulse bit increases as the energy increases. The impulse depends on the discharge current, and the discharge current depends on the energy stored in the capacitor. Figure 6 shows that the maximum impulse bit achieved was 428.3 μN·s when 25 J of energy was used, whereas the minimum impulse bit was 16.13 μN·s when 1.56 J of energy was used at a 15 mm gap. The discharge was indeterminate when 1.56 J of energy was used; thus, 6.25 J (impulse bit: 84.35 μN·s) of energy was used when testing the plasma properties. However, it is worth to note that the calculation of the impulse bit is taken from mathematical manipulation of the current signal to evaluate the electromagnetic contribution of the total impulse bit. The impulse bit calculated in this work does not take into account forces that would occur due to gas dynamics and late time ablation effects, but that can be measured if thrust stand is used. The real impulse bit is estimated to have a tolerance of 10 μN·s.

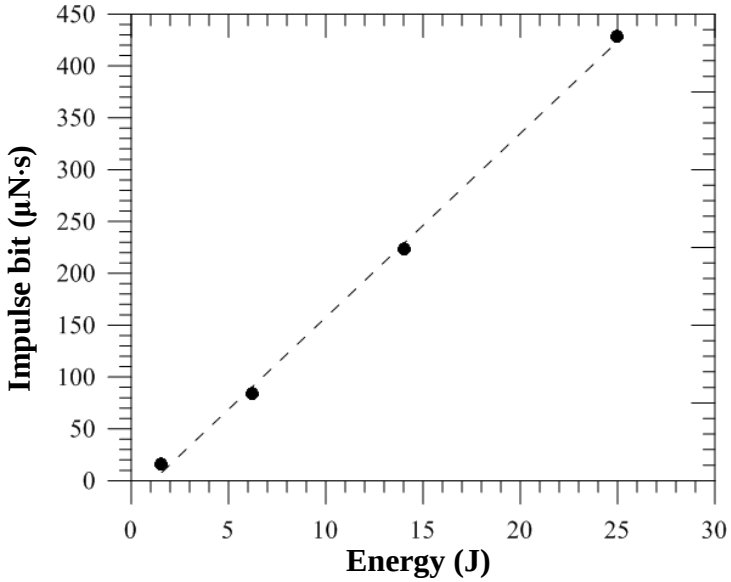

Figure 6 Effect of energy on impulse bit of a thruster at 25 mm electrode gap.

3.2 Electron density measurement

In this test, a 46.5-V battery was used to provide bias voltage between Probes 1 and 2; probe 3 was left to float (Figure 2). The probe (diameter D_i: 0.3 mm; length L: 7 mm) was placed at the exit (30 mm away from the nozzle) of the thruster. When the discharge occurred, the plasma was accelerated out of the thruster toward the triple probe. Probe 1 acted as a positive potential probe; thus, it collected electrons to induce current through the probe, which is measured using a current monitor. The amount of current collected using the positive potential probe, along with the potential difference measured using Probe 3, gives the plasma density. The main discharge current and the amount of current collected by probe 1 are shown in Figure 7. The curve oscillates and exhibits noise because necessary noise-controlling measures were not applied during the test. The current collected using the probe peaked at the peak point of discharge because the Lorentz force was high; consequently, a greater number of electrons are ejected by the thruster (first 18 μs of discharge). When the current direction (from cathode to anode, from 18-36 μs of discharge) changes, the Lorentz force direction did not change; therefore, a second peak in the current was absorbed during the negative peak. This is because that when the current is flowing from anode to cathode (i.e., the current is in the y direction, and the magnetic field is in the z direction so E×B gives positive x direction), the Lorentz force acts on the x direction. When the current is flowing from cathode to anode (the current is in the negative y direction and the magnetic field is in the negative z direction, so E×B still gives positive x direction), the Lorentz force acts on the x direction.

To identify potential differences between Probes 1 and 3, several measurements must be conducted. A voltage probe that is connected to an oscilloscope can ascertain the potential difference with respect to ground. If we use a normal probe connected to an oscilloscope to measure the potential difference between Probes 1 and 3, then Probe 3 is forced to ground. This may induce errors when measuring plasma potential. Furthermore, connecting Probe 3 to ground results in collecting current from the plasma. Thus, using a differential probe, which measures the actual potential difference, or two different probes and measuring Probe 3 with respect to ground on Channel 1 in oscilloscope and measuring Probe 1 with respect to ground on Channel 2 and subtracting both potentials measures the potential difference between Probes 1 and 3. The density with respect to time is obtained and plotted (Figure 8). Figure 8 shows that the maximum density obtained is 8×10^{20} per $m^{3.}$

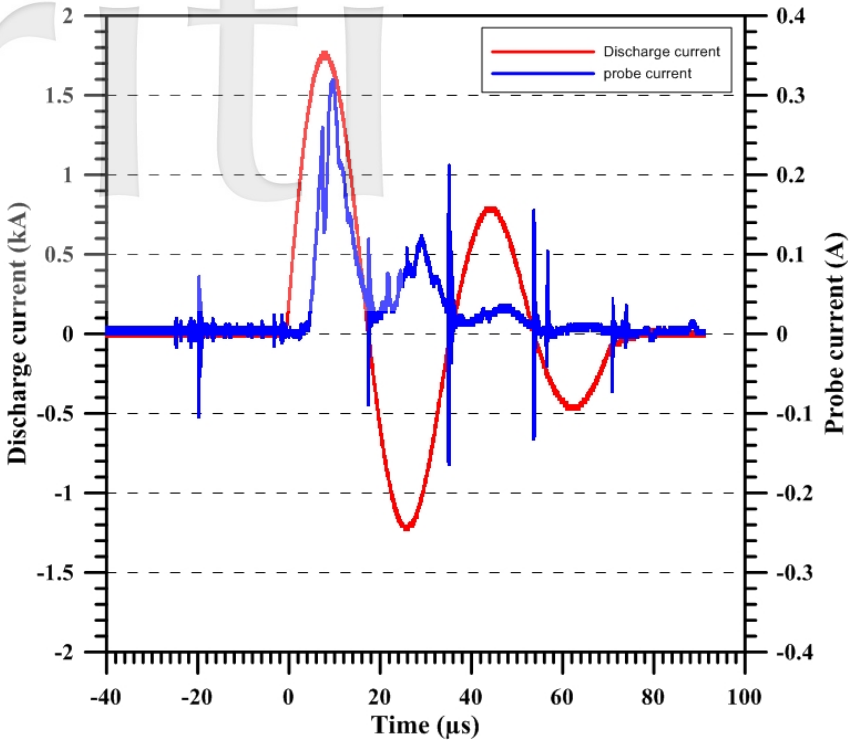

Figure 7 The amount of current collected by Probe 1.

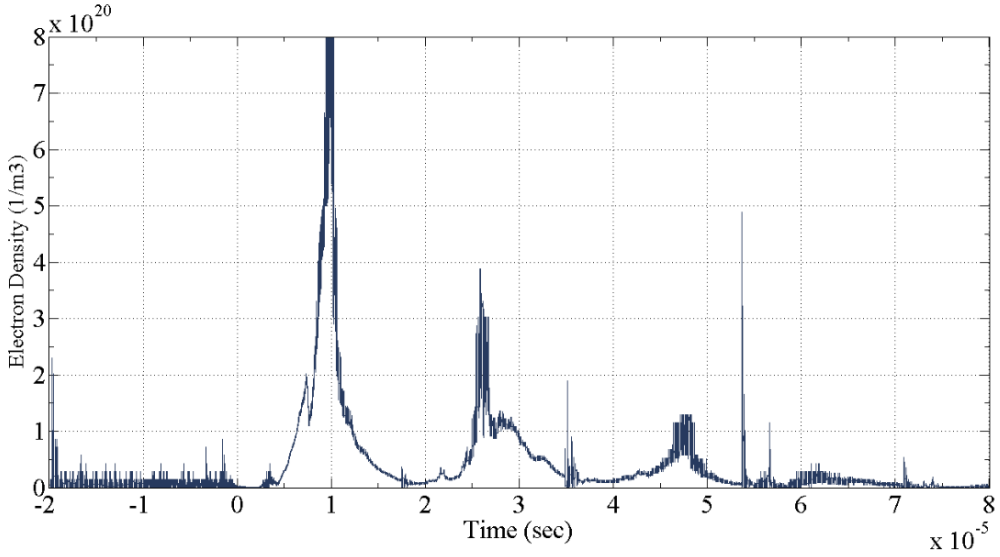

Figure 8 The electron density collected at probe 1.

3.3 Electron velocity measurement

The electron velocity is calculated on the basis of the ToF concept. The Langmuir probe was maintained at various distances from the nozzles. On the basis of the time taken by the electrons to reach the probe and increase the current curve, the electron velocity was defined.

$$V_e = \frac{Distance}{Time\ of\ flight} \quad (12)$$

The probe was placed at three different positions (30, 50 and 70mm) away from nozzle, and the current collected by probe is shown in Figure 9. From Figure 9, the amount of current collected by the probe is decreasing as the probe position is away from the thruster. This is because the plasma is getting neutralized. Electrons were seen moving at an average of 20 km/s.

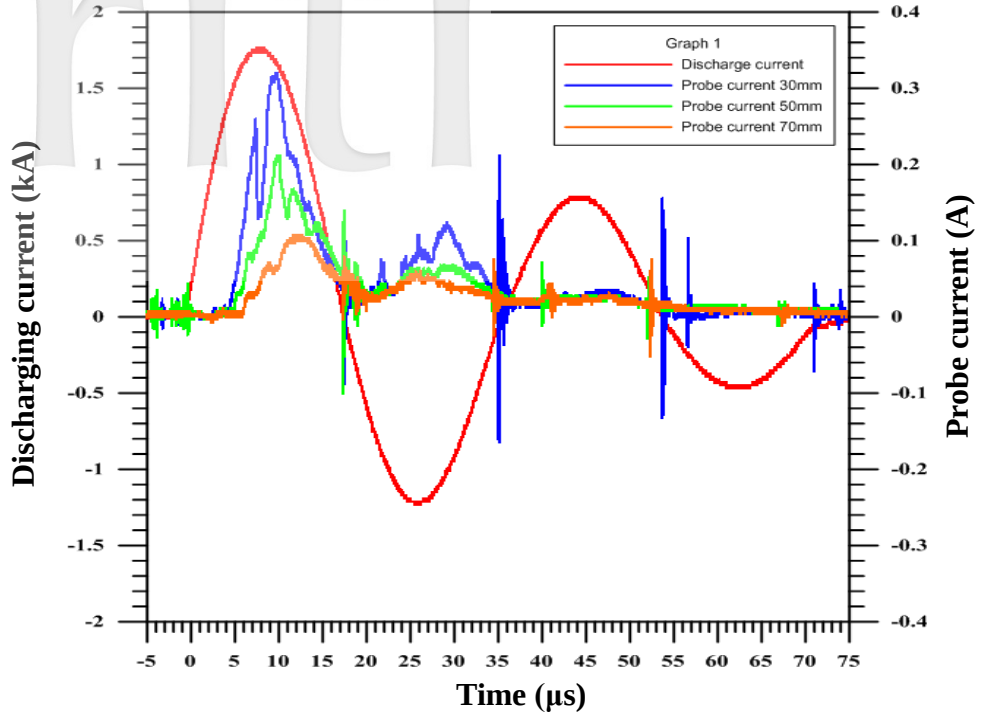

Figure 9 Probe collecting current at different gaps away from nozzle.

3.4 Lorentz force acting on plasma

Figure 10 shows that the discharge duration is 70 μs. A resolution of 256 × 256 pixels at 72 kHz along with an 85-mm Nikon AIS lens (focal length: 1.4) was used to capture the pictures. The aforementioned frame frequency means that the camera captures one image every 14 μs; thus, six images were captured because the total duration was 70 μs (Figure 10). Figure 13a depicts the plasma produced by the spark plug reaching the anode; Figure 10b shows the inception of fuel sublimation on the Teflon surface. In Figure 10b, the discharge occurs at an angle; there are two possible reasons for this. First, the plasma released by the spark plug reaches the anode and creates a discharge. During this process, the electrons travel from the spark plug to the anode. Simultaneously, a Lorentz force is produced by the interaction of the electric and magnetic fields, which acts on the electrons that are moving toward the anode and pushes the electrons toward the exit. However, the current loop must be closed to sustain the discharge, so the electrons pass through the anode at a distance at point 3. These phenomena may result in an angle. The other possibility is that the ions reach the cathode while electrons flow toward the anode. Because the gyro radius of the ions exceeds that of the electrons, more particles and cathodes accumulate. The erosion of the cathode may also lead to more mass accumulating at the cathode, which results in an angle. Subsequently, the spark plug ceases spark production, the electrons from the cathode surface move toward the anode, and a Lorentz force pushes the plasma to the exit (Figure 10c). Figure 10a and b reveal that the plasma accelerates from the middle section to the thruster's nozzle exit and eventually ends in Figure 13d, e, and f. Figure 10g demonstrates the induced Lorentz force ($\boldsymbol{F}$) acting on the plasma and forcing the plasma moving outward.

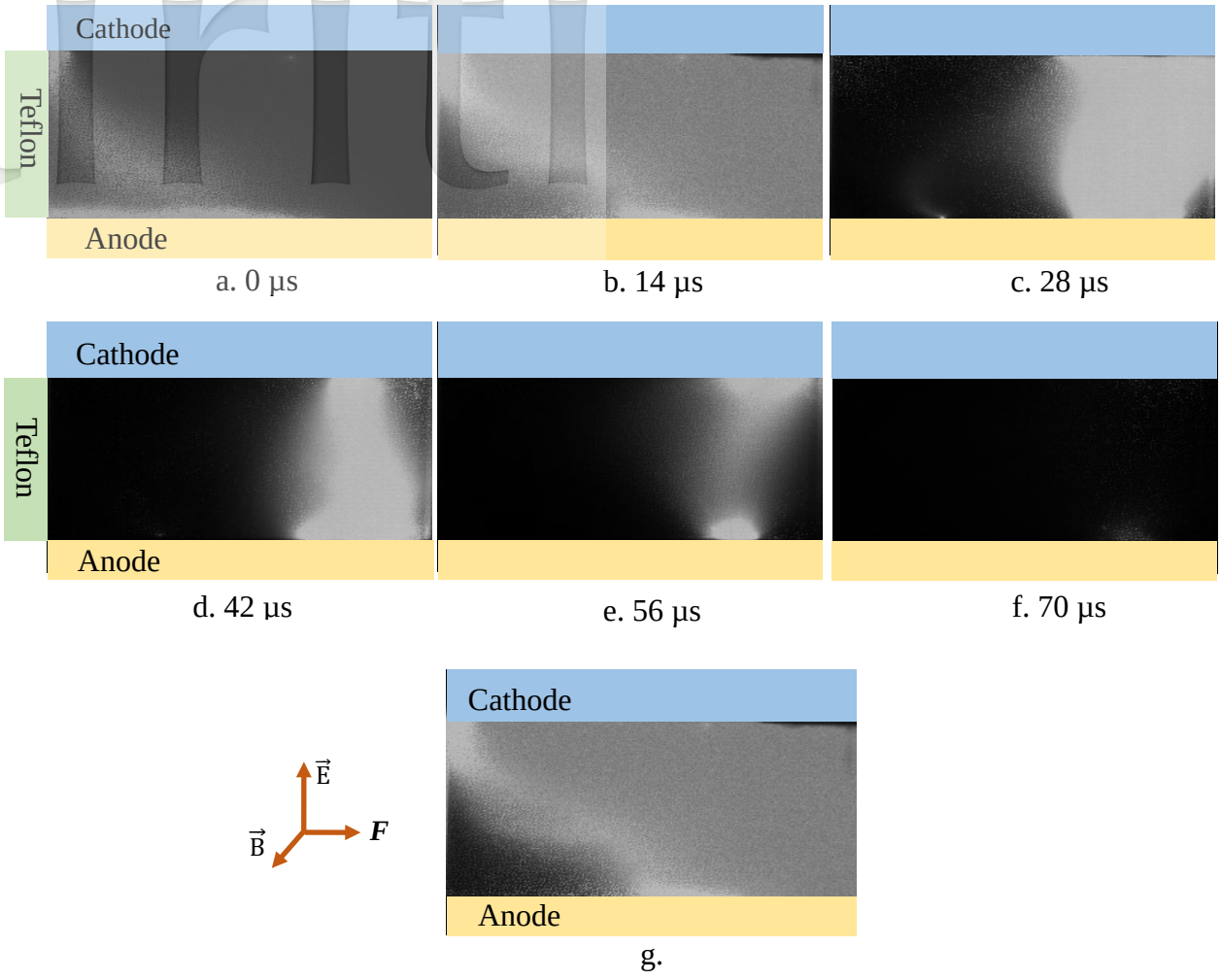

Figure 10 Images (a – f) of discharge from a solid PPT using FASTCAM SA 5 (time lapse: 14μs), and force acting ***F*** on plasma shown in image (g).

IV. CONCLUSIONS

A thruster's impulse was observed to increase as the energy increased; it reached 428.3 μN·s at 25 J when the electrode gap was 25 mm. This is because relatively more energy provides a higher instantaneous current with a substantial Lorentz force. However, to possess high energy, an abundant power source is required; otherwise, substantial time is required to charge the capacitor, which reduces the discharge frequency. A triple Langmuir probe experiment ascertained that the electron density 30 mm from the nozzle was 8×10^{20} m^{-3} when the energy was 6.25 J and the electrode gap was 25 mm. The triple Langmuir probe at various gaps revealed that the peak probe collecting current decreased, which indicated that the density decreased because of the neutral particles neutralizing the plasma. A FASTCAM high-speed camera determined that more particles accumulate at the cathode during the discharge, eventually creating a current sheet canting during discharge.

ACKNOWLEDGMENT

This research was partially supported by the Ministry of Science and Technology under Grant Nos. MOST 104-2221-E-006-136 and MOST 105-2628-E-006-005-MY3.

REFERENCES

[1] Keidar M, et al., "Electromagnetic Effects in the Near Field Plume Exhaust of a Micro-Pulsed-Plasma Thruster," *Journal of Propulsion and Power*, Vol. 20, No. 6, 2004, pp. 961-969.

[2] Kamhawi H, Pencil E, "High Thrust-to-Power Parallel-Rail Pulsed Plasma Thruster Design," in 38th AIAA/ASME/SAE/ASEE Joint Propulsion Conference & Exhibit, 2002, American Institute of Aeronautics and Astronautics.

[3] Nawaz A, et al., "SIMP-LEX: Systematic geometry variation using thrust balance measurements," 30th IEPC, Florence, Italy, 2007.

[4] Palumbo D, Farmingdale N, "Solid propellant pulsed plasma propulsion system development for NS stationkeeping," Electric Propulsion and its Applications to Space Missions, 1981.
[5] Tamura K, "Evaluation of Low Power Pulsed Plasma Thruster for μ-LabSat II," in Proc. 38th AIAA/ASME/ASEE Joint Propulsion Conf. & Exhibit, Indianapolis, USA, July, 2002.
[6] Laystrom J, Burton R, Benavides G, "Geometric Optimization of a Coaxial Pulsed Plasma Thruster," in 39th AIAA/ASME/SAE/ASEE Joint Propulsion Conference and Exhibit, American Institute of Aeronautics and Astronautics, 2003.
[7] Pencil E, Kamhawi H, Arrington L, "Overview of NASA's Pulsed Plasma Thruster Development Program," in 40th AIAA/ASME/SAE/ASEE Joint Propulsion Conference and Exhibit, American Institute of Aeronautics and Astronautics, 2004.
[8] Cooley JE, Choueiri EY, "Fundamentals of PPT discharge initiation: Undervoltage breakdown through electron pulse injection," in 39th AIAA Joint Propulsion Conference. Huntsville, AL. 2003.
[9] Horisawa H, et al., "Plasma Behaviors in a Laser-Assisted Plasma Thruster," in 39th AIAA/ASME/SAE/ASEE Joint Propulsion Conference and Exhibit, 2003.
[10] Scharlemann C, York T, "Alternative Propellants for Pulsed Plasma Thruster," in 38th AIAA/ASME/SAE/ASEE Joint Propulsion Conference & Exhibit, American Institute of Aeronautics and Astronautics, 2002.
[11] Kakami A, et al., "Design and performance of liquid propellant pulsed plasma thruster," *Vacuum*, Vol. 73, No. 3, 2004, pp. 419-425.
[12] Kakami A, et al., "Performance Study on Liquid Propellant Pulsed Plasma Thruster," in 39th AIAA/ASME/SAE/ASEE Joint Propulsion Conference and Exhibit, American Institute of Aeronautics and Astronautics, 2003.
[13] Popov G, et al., "Dynamics and Distribution of Electron Density in the Channel of Pulsed Plasma Thruster," in 38th AIAA/ASME/SAE/ASEE Joint Propulsion Conference & Exhibit, American Institute of Aeronautics and Astronautics, 2002.
[14] Markusic T, et al., "Spectroscopic emission measurements of a pulsed plasma thruster plume," in 33rd Joint Propulsion Conference and Exhibit, American Institute of Aeronautics and Astronautics, 1997.
[15] Nawaz A, et al., "Electrostatic Probe and Camera Measurements for Modeling the iMPD SIMP-LEX," in 43rd AIAA/ASME/SAE/ASEE Joint Propulsion Conference & Exhibit, American Institute of Aeronautics and Astronautics, 2007.
[16] Koizumi H, et al., "Study on Plasma Acceleration in an Ablative Pulsed Plasma Thruster," in 43rd AIAA/ASME/SAE/ASEE Joint Propulsion Conference & Exhibit, American Institute of Aeronautics and Astronautics, 2007.
[17] Parker K, "Pulsed Plasma Thruster plume analysis," *Acta Astronautica*, Vol. 53, No. 4, 2003, pp. 789-795.
[18] Gatsonis N, et al., "Characterization of a Pulsed Plasma Thruster Plume Using a Quadruple Langmuir Probe Method," in 38th AIAA/ASME/SAE/ASEE Joint Propulsion Conference & Exhibit, American Institute of Aeronautics and Astronautics, 2002.
[19] Shaw PV, "Pulsed plasma thrusters for small satellites," University of Surrey (United Kingdom), 2011.
[20] Chen FF, Von Goeler SE, "Introduction to plasma physics and controlled fusion volume 1: Plasma physics," *Physics Today*, Vol. 38, 1985, pp. 87.
[21] Naz MY, et al., "Double and triple Langmuir probes measurements in inductively coupled nitrogen plasma," *Progress In Electromagnetics Research*, Vol. 114, 2011, pp. 113-128.
[22] Eckman R, et al., "Triple Langmuir probe measurements in the plume of a pulsed plasma thruster," *Journal of Propulsion and Power*, Vol. 17, No. 4, 2001, pp. 762-771.
[23] Schönherr T, et al., "Characteristics of plasma properties in an ablative pulsed plasma thruster," *Physics of Plasmas*, Vol. 20, No. 3, 2013, pp. 033503.
[24] Gagne M, et al., "Analysis of triple Langmuir probe measurements in the near-exit region of a gas-fed pulsed plasma thruster," in 35th Joint Propulsion Conference and Exhibit, 1999.
[25] Markusic T, Choueiri E, "Visualization of current sheet canting in a pulsed plasma accelerator," in 26th International Electric Propulsion Conference, Kitakyushu, Japan, 1999.
[26] Chen CT, "Effect of Microwave-induced Plasma on a Flame plasma," 2017.